AIChE

A New Look at Optimal Control of a Batch Crystallizer

Jean-Pierre Corriou
LSGC-CNRS-ENSIC BP20451 54001, Nancy Cedex, France

Sohrab Rohani
Dept. of Chemical and Biochemical Engineering, The University of Western Ontario, London, Ontario, Canada, N6A

DOI 10.1002/aic.11614
Published online October 24, 2008 in Wiley InterScience (www.interscience.wiley.com).

The dynamic optimization of batch crystallizers has been widely studied. A simplified method of optimization inspired from nonlinear model predictive control with a receding horizon is introduced and tested on many different objective functions with various constraints. The proposed optimization method with a receding horizon gives excellent results with no noticeable difference from those obtained by rigorous dynamic optimization and is well adapted to online dynamic optimization. Two different crystallizer models are compared. It is shown that the dynamic optimization problem is constituted of several subproblems related to the constraints on the crystallizer temperature, on the concentration compared to the metastable concentration or on the final moments. Finally, the authors propose simple online control algorithms that result in quasi-optimal temperature profiles provided that the type and sequence of arcs have been previously determined. This method is well adapted to industrial situations. © 2008 American Institute of Chemical Engineers *AIChE J,* 54: 3188–3206, 2008
Keywords: batch crystallizer, quasi-optimal, dynamic optimization, control, model predictive control, receding horizon, robustness

Introduction

Batch crystallization is used as a purification and separation technique in large-scale production of agrochemicals and in high-added value products like pharmaceuticals, proteins, fine chemicals. Batch crystallization despite low investment and easy operation suffers from the lack of reproducibility which affects the purity of the final product. Consequently, the optimal operation of the crystallizers is of major importance for quality and economical reasons. It is often required to suppress spontaneous nucleation and to promote the growth of crystals. In particular, the crystal size distribution (CSD),[1] or its related properties like the mean crystal size and the variance of the CSD must be carefully controlled. Other properties like the morphology of crystals are also important. This is often performed by manipulating the temperature of the slurry (natural cooling, linear cooling, programmed cooling), which influences the driving force of the system, i.e., the supersaturation. Thus, the optimal cooling-supersaturation profile is often sought.[2–9] The seeding policy[10] or the evaporation policy are also important.

The model of the process consists of a set of mass, energy and population balances. The population balance is in the form of a partial differential equation, where the population density depends on time and crystal size. Its solution has attracted many researchers.[9] Among the proposed solutions, the method of classes[11] is often considered as it provides a discrete crystal size distribution. In many cases, the model is based on the application of the method of moments to the population balance equation.[1] The nonlinear dynamic optimi-

Correspondence concerning this article should be addressed to J.-P. Corriou at corriou@ensic.inpl-nancy.fr.

zation problem is set in the open-loop optimal control framework under the Hamilton-Jacobi form or Pontryagin's Maximum Principle.[6] Many techniques can be applied to numerically solve this problem such as control vector parameterization, full state parameterization[7] by means of sequential quadratic programming, or iterative dynamic programming.[12]

An entirely different method compared to previous dynamic optimization techniques is the feedforward control inspired from flatness theory[13] proposed by Vollmer and Raisch.[14] In this approach, a batch crystallizer is shown to be an orbitally flat system and consequently subject to trajectory planning.[15]

The drawback of open-loop policies is that they rely on the model and should take into account the robustness, including model approximation and uncertainties, disturbances and measurement errors. This can be tackled, for example, by the worst-case performance analysis.[16] However, methods which are not based on a model of the process can also demonstrate robustness qualities. Among these, run-to-run methods[17–19] certainly occupy a prominent place. They use the fact that batch processes are repeated and that their outputs, e.g., product quality or characteristics, are often only available at the end of the batch. The information obtained at the end of one run is considered as an output in a discrete feedback control scheme,[20,21] where the independent variable "time" is the counter of performed runs. The quality is thus improved from run to run without the need of on-line measurements. Instead of a model-based framework, it becomes measurement-based.[21] The role of constraints is emphasized as they often determine the solution. In the run-to-run methodology, invariants that characterize the optimal solution despite the presence of uncertainties are identified.[21] They correspond to active terminal constraints and cost sensitivities with respect to input parameters. The solution of the dynamic optimization problem is given by its inputs, i.e., the variables with respect to which the dynamic optimization is performed, which possess the following properties:[19,20]

- The inputs are in general discontinuous,
- Between the discontinuities that occur at switching times, inputs are analytic, and the solution is called an arc,
- Between two successive switching instants, two types of arcs can occur: either an arc determined by a path constraint corresponding to active input bounds or active state constraints, or a sensitivity-seeking arc, where the input remains strictly in the interior of the feasible region limited by the constraints.

The complete optimal profile can thus be parameterized by the type and sequence of arcs, the switching times and variables related to the singular arcs. The invariants correspond to the terminal constraints for the constraint-seeking parameters and to the cost sensitivities for the sensitivity-seeking ones that are not determined by the terminal constraints.[21] The optimization is performed by control of invariants, called generalized constraints. These measurement-based methods considering uncertainty have been gathered under the concept of NCO tracking,[18,22–24] since the necessary conditions of optimality (NCO) are tracked using measurements and the previously determined switching structure corresponding to the optimal solution. NCO conditions are given by these authors under different forms, in particular for run-to-run cases.[18]

In variational calculus, the dynamic optimization problem is classically defined[25,26] as the sum of an algebraic term and an integral term

$$J = G(\boldsymbol{x}(t_f), t_f) + \int_0^{t_f} F(\boldsymbol{x}(t), \boldsymbol{u}(t))dt \tag{1}$$

However, it can be converted[18] to

$$J = \phi(\boldsymbol{x}(t_f), \rho) \tag{2}$$

subject to model equations: $\dot{\boldsymbol{x}} = \boldsymbol{f}(\boldsymbol{x},\boldsymbol{u},\rho)$, initial states: $\boldsymbol{x}(0) = \boldsymbol{x}_0$, path constraints (input or state constraints): $\boldsymbol{S}(\boldsymbol{x},\boldsymbol{u},\rho) \leq 0$, terminal constraints: $\boldsymbol{T}(\boldsymbol{x}(t_f),\rho) \leq 0$. ρ is a vector of parameters, which can include the switching times between the arcs and the final time. The form (2) of the criterion will be retained in the following. According to variational calculus and Hamilton-Jacobi theory, the Hamiltonian based on criterion (1) is defined as

$$H = \lambda^T \boldsymbol{f} + \mu^T \boldsymbol{S} \tag{3}$$

H takes into account the path constraints, λ is the vector of adjoint variables, and μ the vector of Kuhn-Tucker parameters. Thus, the path constraints being included in the Hamiltonian definition, the condition of optimality is that the derivative of the Hamiltonian is equal to zero

$$\frac{\partial H}{\partial \boldsymbol{u}} = \lambda^T \frac{\partial \boldsymbol{f}}{\partial \boldsymbol{u}} + \mu^T \frac{\partial \boldsymbol{S}}{\partial \boldsymbol{u}} = 0 \tag{4}$$

Furthermore, the Jacobi condition writes as

$$\dot{\lambda} = -\frac{\partial H}{\partial \boldsymbol{x}} = -\lambda^T \frac{\partial \boldsymbol{f}}{\partial \boldsymbol{x}} - \mu^T \frac{\partial \boldsymbol{S}}{\partial \boldsymbol{x}} \tag{5}$$

The terminal conditions give

$$\lambda(t_f) = \frac{\partial \phi}{\partial \boldsymbol{x}_f} + \nu^T \frac{\partial \boldsymbol{T}}{\partial \boldsymbol{x}_f} \tag{6}$$

where ν is a vector of Kuhn-Tucker parameters for the terminal constraints in the function

$$\Phi(\boldsymbol{x}(t_f), \rho) = \phi(\boldsymbol{x}(t_f), \rho) + \nu^T \boldsymbol{T}\,(\boldsymbol{x}(t_f), \rho) \tag{7}$$

The Kuhn-Tucker conditions are for the path constraints

$$\mu^T \boldsymbol{S}(\boldsymbol{x}, \boldsymbol{u}, \rho) = 0, \quad \mu \geq 0 \tag{8}$$

and for the terminal constraints

$$\nu^T \boldsymbol{T}(\boldsymbol{x}(t_f), \rho) = 0, \quad \nu \geq 0 \tag{9}$$

The sensitivity conditions are for the path constraints

$$\frac{\partial H}{\partial \boldsymbol{u}} = 0 \tag{10}$$

and for the terminal constraints

$$\frac{\partial \psi}{\partial \rho} = 0 \tag{11}$$

with

$$\psi(\boldsymbol{x}(t_f),\rho) = \Phi(\boldsymbol{x}(t_f),\rho) + \int_0^{t_f} H(t)dt \tag{12}$$

The set of conditions (8–11) is called the necessary conditions of optimality (NCO) by Srinivasan et al.[22]

Other optimization methods claiming to be closer to global optimization include simulated annealing,[3] which requires only the performance index of the process, with no need of gradient information or adjoint equations. Genetic algorithms[5] belong to the same class of optimization methods. However, these stochastic methods are in general very time-consuming and not well suited for online optimization. Simplified algorithms[5] can circumvent this drawback.

In few cases, multiobjective optimization providing the Pareto optimal front is studied even if the problem is of considerable interest. Thus, other variables influencing the final CSD of a batch crystallizer are the initial amount of seed crystals and their size distribution. Simulation studies[3,4,14,27] were performed to determine simultaneously the optimal seeding characteristics and the optimal temperature profile. Sarkar et al[28] studied various multiobjective problems for a seeded batch crystallizer. One example can be to obtain the final CSD with a large mean size and a small coefficient of variation. The approach is based on the use of a genetic algorithm[29] and the determination of the Pareto-optimal solutions. A main drawback of the genetic algorithm method is its high computational demand that cannot be performed for online applications.

Most studies of dynamic optimization for batch or semi-batch crystallizers are performed in simulation and are only applicable offline because of considerable difficulties in obtaining the numerical solution. Moreover, they often do not consider the problems of parameter uncertainty, modelling errors, measurement errors, uncertainty of initial conditions, and the presence of possible disturbances.[30] Consequently, there exists a real need for simpler dynamic optimization methods even if only an approximation to the optimal profile is found. The requirements are that they can be implemented online in a time interval shorter than a sampling period, and that they present robustness qualities. This study deals with single objective dynamic optimization, and intends to develop simple new methods capable of providing quasi-optimal profiles and likely to be easily implemented in the industrial domain.

Dynamic optimization of the crystallizer without heat exchange

A state-space model is used to describe the dynamic behavior of a seeded batch crystallizer. The states x include the concentration C, temperature T, moments μ_i^s with i ranging from 0 to 3 of the seed crystals, and moments μ_i^n of the newly nucleated crystals.

At initial time $t = 0$, the model described by Hu et al[31] is used to initialize the state variables. It is based on a discretization of the partial differential equation

$$\frac{\partial n(r,t)}{\partial t} + \frac{\partial (G(r,t)n(r,t))}{\partial r} = 0 \tag{13}$$

which describes the crystal size distribution.

It is assumed that the growth rate is size-independent, and that there is no fines dissolution. It is equal to

$$G = k_{g0}\,\exp\left(-\frac{E_g}{RT}\right)\left(\frac{C-C_s}{C_s}\right)^g \tag{14}$$

and the nucleation rate

$$B = k_{b0}\,\exp\left(-\frac{E_b}{RT}\right)\left(\frac{C-C_s}{C_s}\right)^b (\mu_3^n + \mu_3^s) \tag{15}$$

C_s is the saturation concentration, and C_m the metastable concentration. A more complicated model including size-dependent growth rate, aggregation, breakage terms, could have been used but would have introduced a large additional complexity,[32] as the model would have been given by a set of partial differential equations, with respect to time and size, and the following method of moments based on a set of ordinary differential equations would not have been applicable. However, it would have no influence on the general methodology which will be developed in the article. Of course, numerically, the results would be slightly different.

If $n(r,t)$ represents the population density, the moments of the crystal-size distribution are defined by

$$\mu_i = \int_0^\infty r^i\, n(r,t)dr \tag{16}$$

All initial moments for the newly nucleated particles μ_i^n are equal to 0 except the zeroth moment μ_0^n which is calculated from the boundary condition

$$n^n(0,t) = \frac{B(t)}{G(0,t)} \tag{17}$$

resulting in

$$\mu_i^n(t=0) = n(0,t) \tag{18}$$

The state-space model of the crystallizer using the moments equations is:

$$\begin{aligned}
&\dot{x}_1 = \dot{C} = -3\,\rho_c\,k_v\,G\,x_4 \\
&\dot{x}_2 = \dot{\mu}_0^s = 0 \\
&\dot{x}_{2+i} = \dot{\mu}_i^s = i\,G\,x_{2+i-1} \qquad i = 1,3 \\
&\dot{x}_6 = \dot{\mu}_0^n = B \\
&\dot{x}_{6+i} = \dot{\mu}_i^n = i\,G\,x_{6+i-1} \qquad i = 1,3 \\
&u = T
\end{aligned} \tag{19}$$

The cooling-rate of the crystallizer is closely related to the temperature profile which is imposed. If isothermal, it is equal to 0. If the profile is piecewise-constant, the temperature is assumed to be constant during a sampling period. It is assumed that the temperature of the crystallizer is perfectly controlled. In real control applications, the optimal temperature profile obtained by dynamic optimization will constitute the set point for the lower level controllers.

Although the aforementioned model is similar to Hu et al,[31] the presentation as a differential system is different. There exist two reasons for not using the discrete model of

Hu et al,[31] but preferentially a continuous differential model. First, in the discrete model used by Hu et al,[31] the discrete equation for concentration

$$x_1^{n+1} = x_1^n - 3\,\rho_c\,k_v\,G\,x_4^n\,\Delta t \tag{20}$$

is of simple Euler-type and may require very small time steps to ensure that the concentration x_1^{n+1} remains positive. This requirement is automatically controlled in a differential equation with a variable-step solver adapted to stiff systems. Secondly, the model based on moments is easier to handle in actual practice when measurements are transformed into state estimations. Finally, it will be shown that the final optimal profile does not change significantly if the population balance of Hu et al,[31,33] or the moments equations are used.

Principle of receding horizon for dynamic optimization

It is well-known that in general dynamic optimization is performed offline due to the large computational effort involved in this operation.[34] It then results in a sub-optimal performance compared to real online dynamic optimization.

In general dynamic optimization consists of finding the solution $\boldsymbol{u}(t)$ of a problem which can be stated as

$$\min_{\boldsymbol{u}(t)} J = G(\boldsymbol{x}(0), \boldsymbol{u}(0), \boldsymbol{x}(t_f), \boldsymbol{u}(t_f)) + \int_0^{t_f} F(\boldsymbol{x}(t), \boldsymbol{u}(t), t)\,dt \tag{21}$$

subject to the equations of the model

$$\dot{\boldsymbol{x}}(t) = \boldsymbol{f}(\boldsymbol{x}(t), \boldsymbol{u}(t))\,; \quad t_0 \le t \le t_f \tag{22}$$

to infinite-dimensional constraints

$$\boldsymbol{p}(\boldsymbol{x}(t), \boldsymbol{u}(t), t) \le 0 \quad \forall t \tag{23}$$

or integral constraints

$$\int_{t_0}^{t_f} q(\boldsymbol{x}(t), \boldsymbol{u}(t), t)dt \le 0 \tag{24}$$

and to terminal constraints

$$\boldsymbol{k}(\boldsymbol{x}(t_0), t_0) = 0\,;\ \boldsymbol{l}(\boldsymbol{x}(t_f), t_f) = 0 \tag{25}$$

This problem can be solved[35] by use of the Hamilton-Jacobi formulation or the Pontryagin's Maximum Principle.[36] The numerical solution to that problem can be obtained by different methods including control vector parametrization,[37] state and control vector parametrization or iterative dynamic programming[12] in discrete time. Often, the optimization is time-consuming and poses difficulties for online optimal control. On-line dynamic optimization should be performed in less than a sampling period. This means that, at each new sampling instant, a new optimal profile needs to be computed, and only the first value of the computed profile will be considered for on-line implementation during the sampling period. If the sampling instant is t, the optimal profile extends from t to the final time t_f. Thus, if the number of sampling periods in the domain $[t, t_f]$ is large, it will result in a large scale optimization problem. Overparameterization of the optimization problem may even result in finding local optima instead of a global optimum. If, furthermore, the dynamic optimization is of nonlinear nature, the problem is likely to be untractable online.

It is proposed here to use the principle of model predictive control[38] or receding horizon for dynamic optimization. The time control horizon is divided into N discrete elements. Assume that the dimension of the control variable is n_u. Instead of considering the optimized variable of the dynamic optimization problem to have dimension $n_u \times N$, the work is performed on a receding horizon of length H_c, and the dimension of the optimized variable, is thus, reduced to $n_u \times H_c$. In principle, the solution obtained by that method should be close to the rigorous solution, as it is known in model predictive control that the control horizon does not need to be large with respect to the prediction horizon. Typically, in linear model predictive control, a control horizon of six sampling periods would be a maximum[39,40] when a prediction horizon can reach more than one hundred sampling periods. However, due to the nature of the problem, the optimization remains nonlinear corresponding to nonlinear model predictive control, where the choice of the control horizon may be more critical.[41] The NLPQL algorithm by Schittkowski[42] is well adapted to numerically solve the nonlinear optimization problem. For a single variable of optimization, when the principle of receding horizon is adopted, at time $t_i = iT_s$ $(i=0, \ldots, n-1)$, with $t_f = nT_s$, the optimization problem is formulated as

$$\min_{\boldsymbol{u}_{k=i,i+H_c-1}} J = G(\boldsymbol{x}(0), \boldsymbol{u}(0), \boldsymbol{x}(t_f), \boldsymbol{u}(t_f)) + \int_0^{t_f} F(\boldsymbol{x}(t), \boldsymbol{u}(t), t)\,dt \tag{26}$$

where the vector to be optimized is $[\boldsymbol{u}_i, \ldots, \boldsymbol{u}_{i+H_{c-1}}]$ for $(i=1, \ldots, n-1)$, and the condition $\boldsymbol{u}_k = \boldsymbol{u}_{i+H_{c-1}}$ for $k = i + H_c, n-1$ traditional in model predictive control is added. The constraints are the same as in Eqs. 23, 24, and 25, however, reformulated in the model predictive discrete formulation.

Studied Problems

Several objective functions have been defined, and in each case the optimal profile has been determined. The initial characteristics for the crystals are the same for all cases.

The seeds are assumed to possess the following crystal size distribution[31,43]

$$n(L^s, 0) = \begin{cases} 0.0032\,(300 - L^s)\,(L^s - 250) & \text{for} \quad 250 \le L^s \le 300\ \mu\text{m} \\ 0 & \text{if } L^s \le 250 \quad \text{or} \quad \le 300 \le L^s \end{cases} \tag{27}$$

The initial values of the states are given in Table 2. The numerical values for the parameters of model (19) are given[31,43] in Table 1. Two bounds are assumed for the temperature of the crystallizer: $T_{\min} = 30°\text{C}$ and $T_{\max} = 50°\text{C}$.

Table 1. Values of the Parameters of the Model

Parameter	Value	Parameter	Value
k_g	1.44×10^8 μm.s^{-1}	k_b	285.0 l.s^{-1}.m^{-3}
E_g/R	4859 K	E_b/R	7517 K
g	1.5	b	1.45
U	1800 kJ.m^{-2}.K^{-1}.h^{-1}	A	0.25 m^2
ΔH	44.5 kJ.kg^{-1}	C_p	3.8 kJ.kg^{-1}.K^{-1}
M	3 kg (Hu et al[31])	ρ_c	2.66×10^{-12}g.μm^3
	27 kg (Sarkar et al[28])	k_v	1.5

The saturation and metastable concentrations are respectively related to the temperature (in Celsius) by the following equations

$$C_s(T) = 6.29 \times 10^{-2} + 2.46 \times 10^{-3}\, T - 7.14 \times 10^{-6}\, T^2$$
$$C_m(T) = 7.76 \times 10^{-2} + 2.46 \times 10^{-3}\, T - 8.10 \times 10^{-6}\, T^2 \tag{28}$$

For each simulation, a sampling period equal to $T_s=36$ s is chosen in general, i.e., the manipulated input will be piecewise-constant on a sampling period. The final time t_f is fixed and equal to 1,800 s, i.e., 50 sampling periods. During the first sampling period from $t = 0$ to $t=T_s$, the maximum temperature is imposed yielding the initial crystallizer temperature profile, the ordinary differential equations of the system are integrated in this time interval. The reason of this choice lies in the fact that in actual practice the dynamic optimization will start in this time interval $[0, T_s]$, and the first applied input will occur at $t=T_s$. In simulation, the dynamic optimization starts at discrete time k $(k \geq 1)$, the calculated optimal manipulated input $u=T(k)$ is applied, the ordinary differential equations integrated from k to $k + 1$, and the process is repeated. In the case where "online" dynamic optimization is performed in the spirit of model predictive control, at time $t_i=iT_s$ $(i=1,\ldots,N-1)$, H_c values of T are computed: $T(k)$ for $(k=i,\ldots,i+H_c-1)$, and the following values of T are assumed to be equal to the last optimized value: $T(k)=T(i+H_c-1)$ for $(k=i+H_c,\ldots,N-1)$. Thus, the control horizon H_c will be varied between $H_c=3$ (corresponding to a small horizon) and full horizon $H_c=N-1-i$, such that the last optimized temperature is $T(N-1)$ at time t_i. There is no need for optimization at final time t_N as the last input implemented $T(N-1)$ will be active on the last time interval $[t_{N-1}, t_N]$. The full horizon is considered as the reference of classical dynamic optimization and, for the receding horizon strategy, the control horizon is first chosen small, then increased if necessary. The dynamic optimization based on model predictive control or receding horizon is well adapted for online operation as it can take into account the actual measurements at each sampling instant. A state estimator such as an extended Kalman filter or a receding horizon observer[35] can also be used to estimate the unmeasured states.

The programs have been written in Fortran. The integration code for the ordinary differential equations is LSODA well adapted for stiff systems,[44,45] and NLPQL is chosen for nonlinear optimization.[42] In all cases, the relative tolerance for the integrator LSODA was chosen equal to 10^{-8}, and the tolerance for the nonlinear optimizer NLPQL was chosen equal to 10^{-12}. At these levels, no noticeable improvement of the numerical results was noted by reducing these tolerances.

Case 1 The optimization problem with respect to crystallizer temperature is

$$\min_{T(t)} J = \mu_3^n(t_f) - \mu_3^s(t_f) \tag{29}$$

subject to model equations (19), initial conditions, constraints (30) and (31). The objective of this criterion is to minimize the size of newly nucleated crystals, while maximizing the size of crystals growing from the initial seeds.[31] Active nonlinear constraints are set so that the concentration remains between the saturation and metastable concentrations at any time

$$C_s \leq C \leq C_m \tag{30}$$

It is, furthermore, assumed that the optimal temperature cannot increase with time

$$\frac{dT}{dt} \leq 0 \tag{31}$$

which is a linear constraint for the discrete optimization problem.

Compared to the optimal profiles resulting from the full optimization (Figure 1) and to those published by Hu et al,[31] the optimal profiles (Figure 2) calculated according to the simplified procedure described in the principle of receding horizon for dynamic optimization coincide very well.

When the control horizon is varied (Table 3), very close temperature profiles are obtained with values of the receding horizon $H_c=5, 10$, even with $H_c=3$, this latter with a very slight deviation, compared to the temperature profile calculated with full horizon and denoted by "one pass". "One pass" corresponds to a single optimization instead of a sequence of optimizations in the case of the receding horizon, each one after the success of the previous iteration. It does not mean that the iterative calculation takes a longer time than the calculation performed with full control horizon ("one pass"). This characteristics is due to the fact that in "one pass", the number of optimization variables is larger than with a shorter control horizon. Moreover, it appears that indeed the control horizon H_c has practically no influence on the optimal crystallizer temperature profile, and even less on the value of the optimal criterion. The optimal temperature profile is such that the crystal concentration is equal to the metastable concentration corresponding to upper constraint (30), however, as the metastable concentration is related to the temperature by (28), which can be represented under the general form

Table 2. Initial Values of the States and Input of the Model

State	Value	State	Value
$x_1=C$	0.1743 g solute/g solvent		
$x_2=\mu_0^s$	66.66	$x_6=\mu_0^n$	0.867
$x_3=\mu_1^s$	1.83×10^4	$x_7=\mu_1^n$	0
$x_4=\mu_2^s$	5.05×10^6	$x_8=\mu_2^n$	0
$x_5=\mu_3^s$	1.93×10^9	$x_9=\mu_3^n$	0
Input $u = T$	50°C		

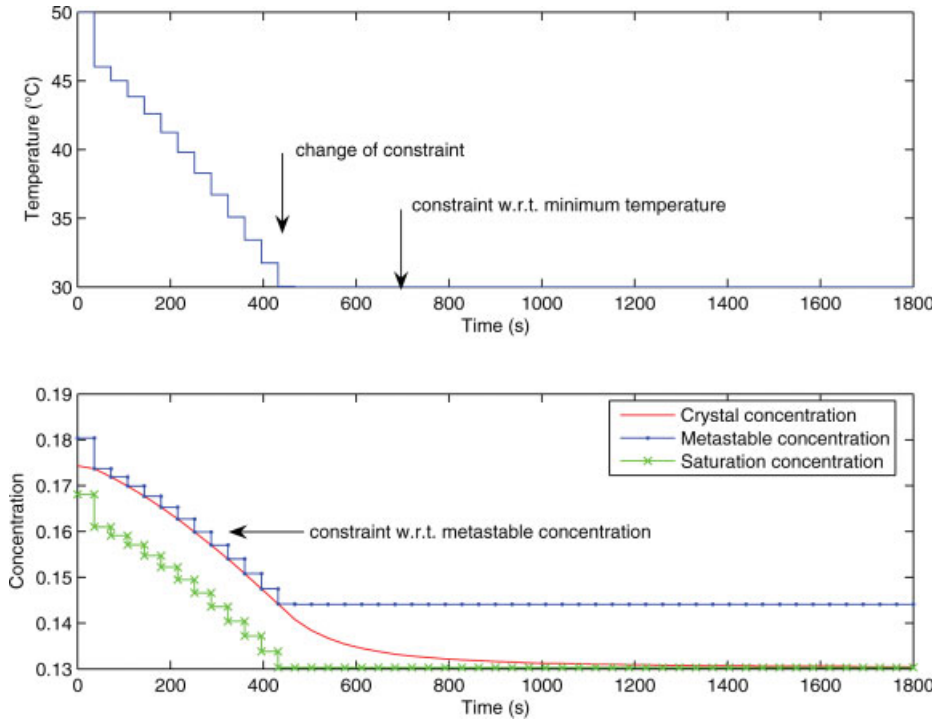

Figure 1. Optimal temperature profile (top), and resulting concentration profile (bottom), computed by "online" dynamic optimization in one pass with evidence of constraints (Objective function: $J=\mu_3^n(t_f)-\mu_3^s(t_f)$).

[Color figure can be viewed in the online issue, which is available at www.interscience.wiley.com.].

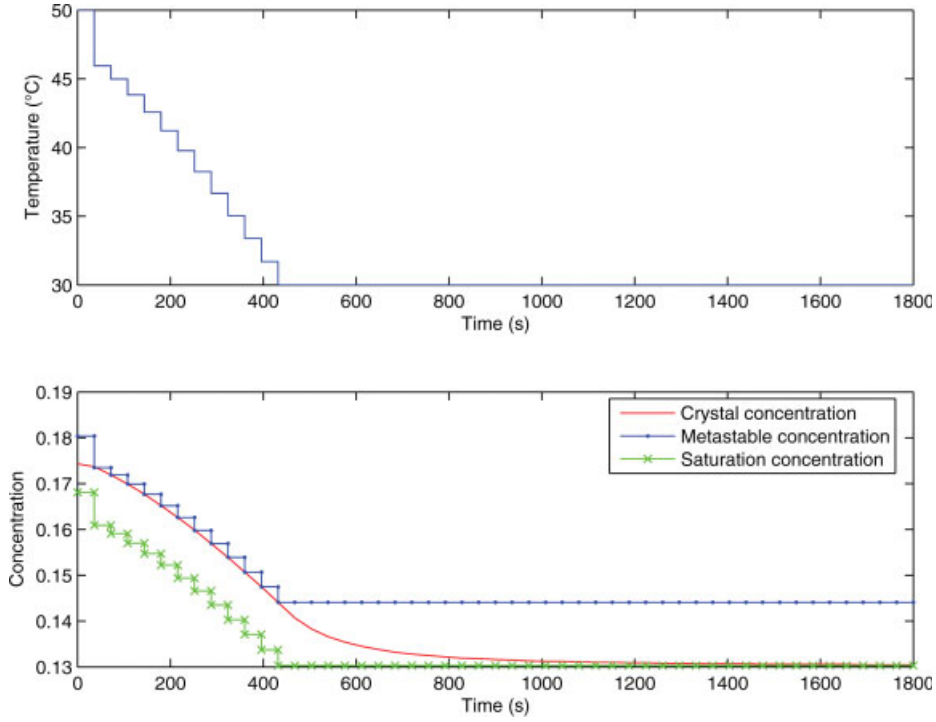

Figure 2. Top: Optimal temperature profile computed by 'online' dynamic optimization with a receding horizon equal to 3. Bottom: corresponding concentration profile (Objective function: $J=\mu_3^n(t_f)-\mu_3^s(t_f)$).

[Color figure can be viewed in the online issue, which is available at www.interscience.wiley.com.]

Table 3. $J=\mu_3^n(t_f)-\mu_3^s(t_f)$. Influence of the Control Horizon on the Optimal Profile of Temperature and on the Value of the Criterion

Time t	T (H_c = 3)	T (H_c = 5)	T (H_c = 10)	T (one pass)
0.000	50.0000	50.0000	50.0000	50.0000
36.000	45.9508	46.0282	46.0282	46.0282
72.000	44.9846	45.0002	45.0041	45.0041
108.000	43.8349	43.8579	43.8588	43.8587
144.000	42.5747	42.6018	42.6027	42.6023
180.000	41.2156	41.2470	41.2480	41.2468
216.000	39.7704	39.8063	39.8063	39.8051
252.000	38.2520	38.2925	38.2930	38.2906
288.000	36.6731	36.7184	36.7190	36.7161
324.000	35.0458	35.0957	35.0963	35.0935
360.000	33.3928	33.4355	33.4363	33.4334
396.000	31.7040	31.7480	31.7487	31.7454
432.000	30.0000	30.0418	30.0425	30.0372
468.000	30.0000	30.0000	30.0000	30.0000
$\mu_3^s(t_f)$	1.237×10^{10}	1.237×10^{10}	1.237×10^{10}	1.237×10^{10}
$\mu_3^n(t_f)$	2.585×10^{9}	2.586×10^{9}	2.586×10^{9}	2.586×10^{9}
Criterion $\mu_3^n(t_f)$ $-\mu_3^s(t_f)$	-9.785×10^{9}	-9.784×10^{9}	-9.784×10^{9}	-9.784×10^{9}

$$C_m = g(T) \tag{32}$$

Thus, the optimal temperature of the crystallizer results implicitly, provided that this temperature is between the maximum and minimum temperatures of the crystallizer. The coincidence of the crystal concentration, and of the metastable concentration can be verified as well in Figures 1 for one pass as in Figure 2, for a very low value of $H_c=3$, and in Figure 4a of Hu et al.[31] When the temperature meets the minimum temperature, it remains constant at that minimum value.

Thus the optimal temperature profile consists of two arcs separated by one switching time t_1^{sw}:

1. An arc corresponding to the metastable concentration constraint $C=C_m(T)$ (state constraint, also called path constraint) on $[0, t_1^{sw}]$,
2. An arc corresponding to the lower input bound (input constraint) on $[t_1^{sw}, t_f]$.

Thus, for the objective function considered, the optimal temperature profile results from two constraints, first the constraint on the concentration being equal to the metastable concentration, secondly the temperature being equal to the minimum temperature. The temperature is the optimization variable and the constraints are of different nature for the dynamic optimization problem. The constraints with respect to the concentration are nonlinear and implicitly depend on the optimization variable, whereas the constraints with respect to the temperature are simply linear with respect to the optimization variable. This is shown in Figure 1. Having determined these two constraints, the time at which the controller has to switch from one constraint to another constraint must be found. The instant of switching can be simply found as the time when the decreasing temperature of the crystallizer meets the minimum temperature.

Case 2 The optimization problem with respect to crystallizer temperature is

$$\min_{T(t)} J = \mu_3^n(t_f) \tag{33}$$

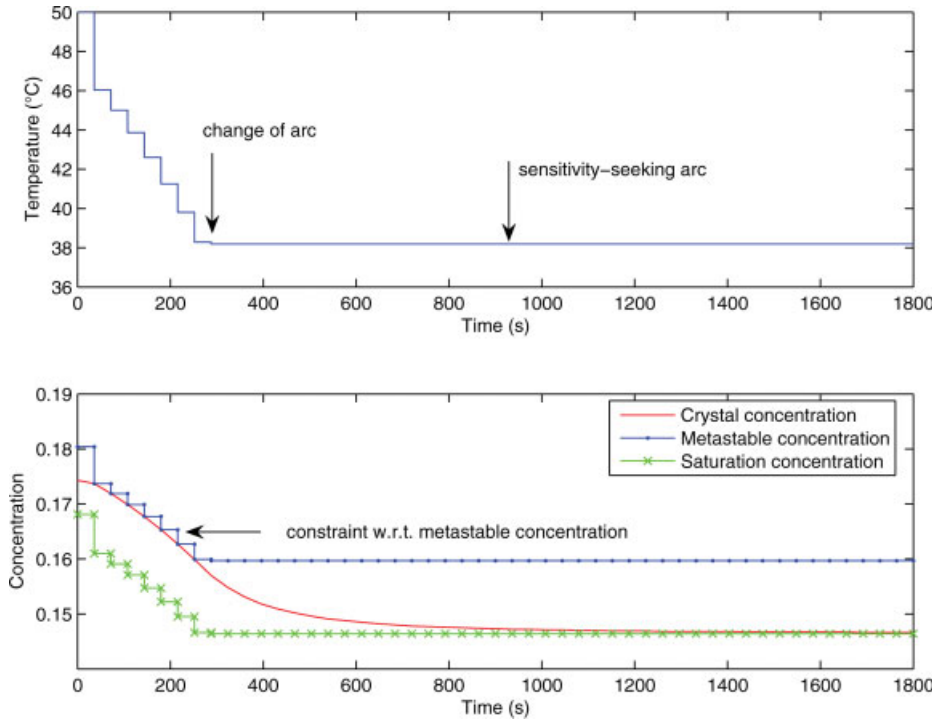

Figure 3. Top: optimal temperature profile computed in one pass. Bottom: resulting concentration profiles (Objective function: $J=\mu_3^n(t_f)$ submitted to constraint $\mu_3^s(t_f)\geq 8.33\times10^9$).

[Color figure can be viewed in the online issue, which is available at www.interscience.wiley.com.]

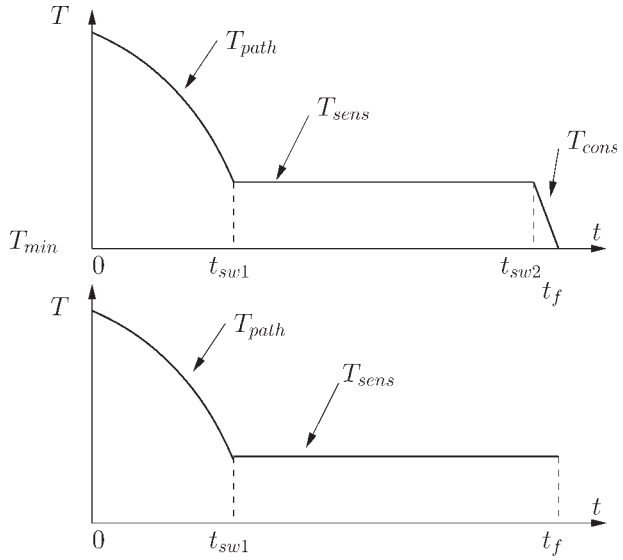

Figure 4. Scheme of two possible profiles for cases 2 and 3: top with a sensitivity-seeking arc, and a final constraint-seeking arc (study of Hu et al[31] with a continuous profile), bottom with one sensitivity-seeking arc (this study with a piecewise-constant profile).

subject to model equations (19), initial conditions, constraints (30), (31) and (34). This objective function aims at minimizing only the size of newly nucleated crystals.[31,43] The nonlinear constraint (30) for the concentration and the linear constraint (31) for the decrease of temperature are still valid. Another nonlinear constraint is that the final third moment for the seeded particles is above a given value

$$\mu_3^s(t_f) \geq 8.33 \times 10^9 \tag{34}$$

The optimal temperature profile (Figure 3) clearly shows two parts: the first one where the optimal temperature of the crystallizer decreases so that the constraint with respect to the metastable concentration is satisfied, the second one where it remains at a constant temperature. Hu et al[31] found a very similar plateau followed by a final decrease to the minimum temperature; however, their conditions of optimization are slightly different, the numerical values for these temperatures and for the numerical tolerances that they used are not known. Furthermore, they computed continuous profiles starting at $t=0$ and ending at $t=t_f$, whereas our profiles are piecewise-constant and start at first sampling time T_s. On the basis of first results such as given by Hu et al,[31] the optimal profile could be thought to be composed of three arcs as shown in Figure 4. The first arc resulting from the path constraint (30) is fairly obvious and exactly similar to case 1. The second arc present on $[t_{sw1}, t_{sw2}]$ (Figure 4, top) is a sensitivity-seeking arc as no path or input constraint is satisfied along this arc. The third arc on $[t_{sw2}, t_f]$ would also be a constraint-seeking arc aiming at satisfying the final constraint. However, in our case of a piecewise-constant profile, repeated simulations with careful examinations of the numerical results and observation of numerical tolerances have shown that the second and third arcs are not distinguishable in most optimizations (Figure 4, bottom), both for the present case 2 or case 3 that will be studied in the following. The main point is that the temperature on $[t_{sw1}, t_f]$ can be considered as constant. If there may be a numerical decrease toward the final time in some cases (refer to Table 6 for case 3), this decrease is so small (often lower than 0.01K) that it is very difficult to attribute it to a different interpretation. The results that are shown here by the receding horizon or one pass dynamic optimizations presented before have been confirmed by use of a different dynamic optimization approach, i.e., the control vector parameterization (CVP) method performed exactly as recommended by Goh and Teo,[37,46] which has been applied on the same studied cases. The main difference with the one pass dynamic optimization here performed is that the path constraints are considered as continuous constraints in CVP instead of being considered only at the grid points in the present method. The gradients have been calculated by two methods: finite differences and sensitivity analysis,[47,48] which gave similar results, however, the use of sensitivities considerably slowed the calculations without any numerical improvement.

In summary, in this case, the optimal temperature profile consists of two arcs separated by one switching point:

1. An arc corresponding to the metastable concentration constraint $C=C_m$ (state constraint) on $[0, t_1^{sw}]$,
2. A sensitivity-seeking arc on $[t_1^{sw}, t_f]$.

Srinivasan et al[17] propose a method to find the values of u_{path} and u_{sens}, and apply it to a number of physical cases. In our case, u_{path} results from inversion of Eq. 32. The problem of u_{sens} (see also Logsdon and Biegler[26]) is more difficult. On the sensitivity-seeking arc, no constraint is active, so that the Hamiltonian is reduced to

$$H=\lambda^T \boldsymbol{f} \tag{35}$$

and the condition of optimality is

$$H_u = \frac{\partial H}{\partial u} = \lambda^T \frac{\partial \boldsymbol{f}}{\partial u} = 0 \tag{36}$$

In nonlinear geometric control,[49] which deals with systems which are affine with respect to the input, i.e., which are expressed under the form

$$\dot{\boldsymbol{x}} = \boldsymbol{F}(x) + \boldsymbol{G}(x)\boldsymbol{u} \tag{37}$$

the manipulated input is obtained in analytical form by considering the successive derivatives of the input until the relative order is reached. In a way similar to that method, even if is not restricted to systems affine with respect to the input, Srinivasan et al[17] propose to differentiate the partial derivative H_u with respect to time. The first derivative is equal to

$$\frac{dH_u}{dt} = \lambda^T \Delta \boldsymbol{f}_u = \lambda^T \left(\frac{\partial \boldsymbol{f}_u}{\partial \boldsymbol{x}} \boldsymbol{f} - \frac{\partial \boldsymbol{f}}{\partial \boldsymbol{x}} \boldsymbol{f}_u + \frac{\partial \boldsymbol{f}_u}{\partial \boldsymbol{u}} \dot{\boldsymbol{u}}\right) \tag{38}$$

then using this operator Δ, time differentiations are performed until u appears in $\lambda^T \Delta^i \boldsymbol{f}_u$. The input would, thus, result as depending on the states $\boldsymbol{x}$ and on the adjoint variables λ. To avoid the dependence on λ, Srinivasan et al[17]

Table 4. $J=\mu_3^n(t_f)$. Influence of the Control Horizon on the Optimal Profile of Temperature

Time t (s)	T (H_c = 15)	T (H_c = 20)	T (one pass)
0	50.0000	50.0000	50.0000
36	46.0282	46.0282	46.0282
72	45.0041	45.0041	45.0041
108	43.8588	43.8588	43.8588
144	42.6027	42.6027	42.6027
180	41.2480	41.2480	41.2480
216	39.8073	39.8073	39.8073
252	38.2936	38.2936	38.2936
288	38.1881	38.1881	38.1878
⋮	⋮	⋮	⋮
t_f = 1800	38.1881	38.1881	38.1878
Final moment $\mu_3^s(t_f)$	8.330×10^9	8.330×10^9	8.330×10^9
Final moment $\mu_3^n(t_f)$ (criterion)	7.7653×10^8	7.7653×10^8	7.7658×10^8

Final values of the moments and of the criterion are also given.

introduce the matrix $\mathcal{M} = [\, \boldsymbol{f}_u; \Delta \boldsymbol{f}_u \ldots \Delta^i \boldsymbol{f}_u]$ for $i=1,\ldots,m$; m being the dimension of the state-space reached by manipulation of u. By using the condition of the rank of $\mathcal{M}$ lower than its structural rank, the control u can be obtained.

In our case, we tried to use the same ideas and the input u appears explicitly already in $H_u = \lambda^T \boldsymbol{f}_u = 0$. However, our attempts to find an analytical solution failed for two reasons. First, the system (19) is far from being affine with respect to the input, second the dimension of the system is much larger than the simple examples of Srinivasan et al.[17] The first reason explains why the explicit analytical inversion of the mathematical expressions could not be obtained.

The optimal profiles have been computed with different values of the control horizon. It was found that the influence of the control horizon was much more important than in the previous dynamic optimization of case 1. Figure 3 represents the results from dynamic optimization performed in "one pass". Table 4 shows the influence of the control horizon on the optimal profiles of temperature. When the control horizon becomes sufficiently large, the plateau temperature is nearly the same. In fact, the plateau temperature corresponds exactly to the temperature leading to the satisfaction of the inequality constraint (34). Optimization with receding horizons $H_c=5$ and $H_c=10$ did not yield satisfactory results, which reveals a more difficult optimization than for case 1, where the use of $H_c=3$ was sufficient to obtain a profile very close to the optimal one. For a receding horizon $H_c=15$, the constraint (34) is exactly satisfied, and the values of the criteria are very close to the profile obtained by full dynamic optimization.

When the results of the final moments are compared for case 1 (Table 3), and case 2 (Table 4), it appears that in case 1, the value of moment $\mu_3^s(t_f)$ is larger than in case 2, and fulfills the constraint (34) of case 2, but this is at the price of a larger moment undesirable $\mu_3^n(t_f)$ corresponding to the criterion of case 2. The consequence is that the requirement in case 2 is the satisfaction of the constraint (34), which prevents the temperature of decreasing to its lower bound.

Case 3 The optimization problem with respect to crystallizer temperature is

$$\min_{T(t)} J = \frac{\mu_3^n(t_f)}{\mu_3^s(t_f)} \tag{39}$$

subject to model Eq. 19, initial conditions, constraints (30), (31) and (40). This objective function is formulated differently from that of case 1, but similarly aims at minimizing the size of newly nucleated crystals, while maximizing the size of crystals growing from the initial seeds Hu et al.[33] The nonlinear constraint (30) for the concentration, and the linear constraint (31) for the decrease of temperature are again valid. Furthermore, the final third moment for the seeds is larger than a given value $\mu_{3,\min_f}^s$

$$\mu_3^s(t_f) \geq \mu_{3,\min_f}^s \tag{40}$$

The influence of the optimization method has been first studied for $\mu_3^s(t_f) \geq 5 \times 10^9$. For optimization based on a receding horizon strategy, there is practically no influence of the control horizon ($H_c=3, 5, 10$ or 20) on the graphical and even numerical results (Table 5). When the optimization is performed in one pass, the main difference with the results from the optimization, based on a receding horizon strategy, is that the "one pass" optimization is difficult, whereas the receding horizon optimization poses no problem and is much faster. For the "one pass" optimization, to avoid failures, an initial temperature profile close to the final optimal profile was chosen as an optimal profile resulting from a receding horizon optimization, and later randomly perturbed by an additive noise of uniform probability density function. The profiles of optimal temperatures for "one pass" and receding horizon optimizations (Figure 5) show no visible difference. The comparison of the seeds third moments (Figure 6) shows that both satisfy exactly the final constraint taken as an equality. Finally, the evolution of the criteria has been also compared for these two cases (Figure 6). Again, the difference is not visible on the figures between the "one pass" and receding horizon strategies.

When the number of steps is increased from 10 to 100, the piecewise-constant profiles tend progressively (Figure 7) toward a continuous profile but the plateau temperature remains nearly unchanged.

In Table 6, the comparison has been performed for different values of the constraint on $\mu_3^s(t_f)$. When the value of $\mu_{3,\min_f}^s$ is increased to $\mu_{3,\min_f}^s = 7 \times 10^9$ and $\mu_{3,\min_f}^s = 9 \times 10^9$, the optimization becomes progressively more difficult even for the receding horizon optimization and fails in many cases unless the previously mentioned precautions about initial profiles are taken. The influence of the value of the constraint

Table 5. $J=\mu_3^n(t_f)/\mu_3^s(t_f)$. Influence of the Value of the Control Horizon on the Criterion for the Constraint Value $\mu_{3,\min_f}^s = 5 \times 10^9$ and comparison with One Pass Optimization Initialized by a Perturbed Profile Resulting from $H_c=10$ Optimization

Horizon H_c	T at level	Criterion $\frac{\mu_3^n(t_f)}{\mu_3^s(t_f)}$	Final constraint $\mu_{3,\min_f}^s$
3	45.3114	0.025125	5.000×10^9
5	45.3111	0.025167	5.000×10^9
10	45.3111	0.025167	5.000×10^9
20	45.3114	0.025125	5.000×10^9
one pass	45.3101	0.025134	5.001×10^9

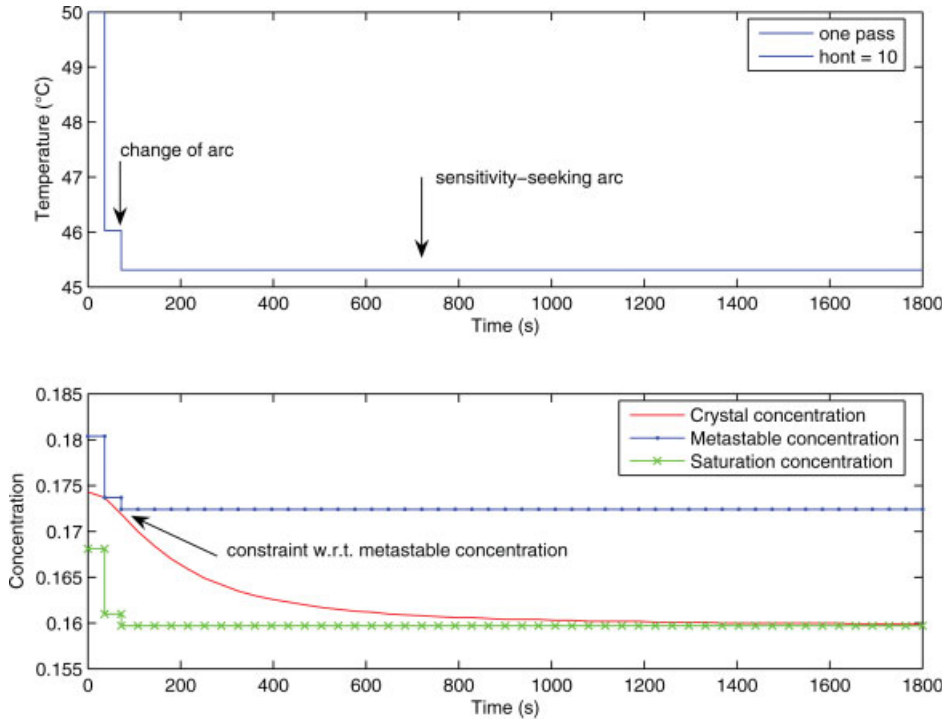

Figure 5. Top: comparison of optimal temperature profile computed in one pass and with receding horizon strategy (H_c=10). Bottom: resulting concentration profiles (Objective function: $J=\mu_3^n(t_f)/\mu_3^s(t_f)$ submitted to constraint $\mu_3^s(t_f) \geq 5 \times 10^9$).

[Color figure can be viewed in the online issue, which is available at www.interscience.wiley.com.]

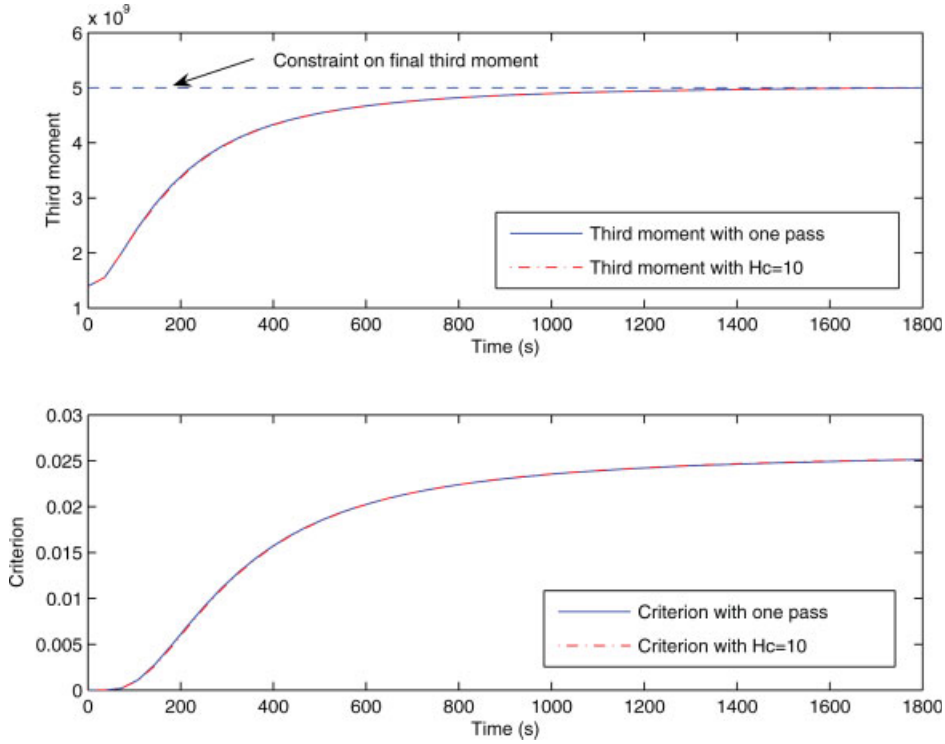

Figure 6. Top: comparison of the profiles of the third seed moments computed in one pass and with receding horizon strategy. Bottom: Comparison of the profiles of the criteria computed in one pass and with receding horizon strategy (Objective function: $J=\mu_3^n(t_f)/\mu_3^s(t_f)$ submitted to constraint $\mu_3^s(t_f) \geq 5 \times 10^9$).

[Color figure can be viewed in the online issue, which is available at www.interscience.wiley.com.]

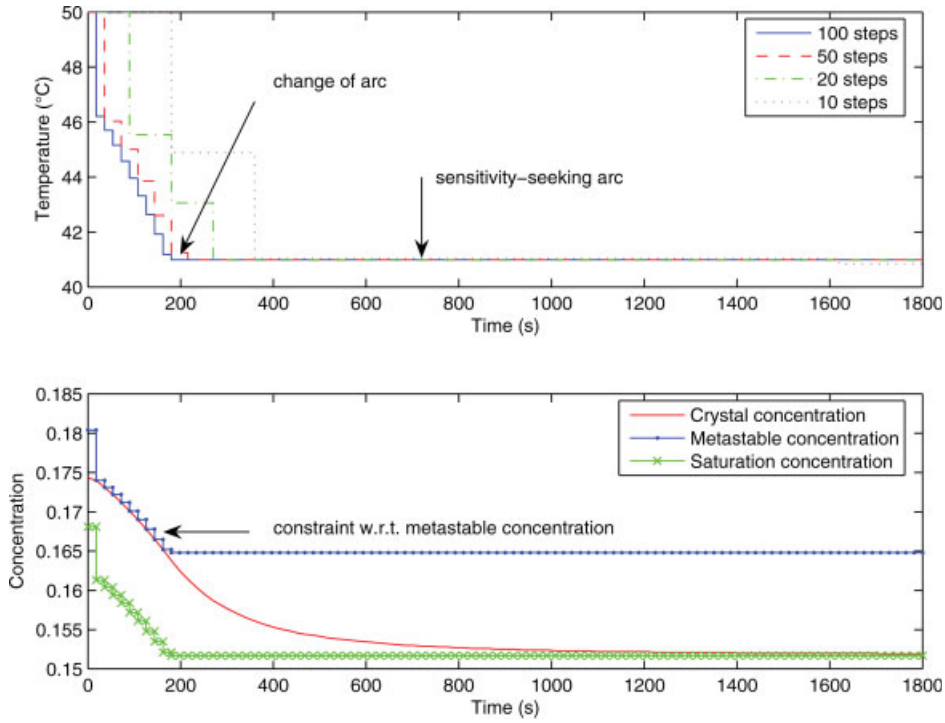

Figure 7. Top: optimal temperature profiles computed in one pass for different numbers of steps. Bottom: resulting concentration, saturation and metastable concentrations with 100 steps (Objective function: $J=\mu_3^n(t_f)/\mu_3^s(t_f)$ submitted to constraint $\mu_3^s(t_f) \geq 7 \times 10^9$).

[Color figure can be viewed in the online issue, which is available at www.interscience.wiley.com.]

$\mu^s_{3,\min,f}$ ($\mu^s_{3,\min,f}=3,5,7$ or 9×10^9) on the optimal profile is shown in Figure 8. The temperature profiles present similar characteristics and only differ by the switching time between the first path constraint arc corresponding to the constraint with respect to the metastable concentration, and the second sensitivity-seeking arc which is determined by the value of the final constraint.

For receding horizon optimization, increasing the length of the horizon generally suffices to obtain satisfactory results. For full horizon optimization, the initialization of the temperature profile as the maximum available temperature generally fails and leads to solutions which have a worse value of the criterion than in case of receding horizon. In this case, a good solution is again obtained by initializing the temperature profile as the sum of an optimal profile resulting from the receding horizon optimization and a noise of uniform distribution with $\sigma=0.5$. Thus, it is likely that the optimization problem presents several extrema, and that the solution gets frequently trapped into a local minimum. However, it must be noted that the value of the criterion from "one pass" optimization is not better than the one obtained by receding horizon optimization. Another successful solution for the "one pass" optimization is to start the optimization with a relatively small number of time increments in order to decrease the number of optimization variables and then to start from a successful temperature profile and increase progressively the number of time increments (Table 7 gathers such results in the case where $\mu^s_{3,\min,f}=7\times10^9$).

At final time, the optimal profile (Figure 5) results in the transformation of the inequality constraint (40) into an equality constraint (Figure 6). In this case, again the optimal temperature profile consists of two arcs separated by one switching point:

1. An arc corresponding to the metastable concentration constraint $C=C_m$ (state constraint) on $[0, t_1^{sw}]$,
2. A sensitivity-seeking arc on $[t_1^{sw}, t_f]$.

From that point of view, cases 2 and 3 are identical even if the objective function differs.

Table 6. $J=\mu_3^n(t_f)/\mu_3^s(t_f)$. Influence of the Value of the Constraint (40) on the Level Temperature, on the Final Value of $\mu_3^s(t_f)$ and on the Criterion

Constraint $\mu^s_{3,\min,f}$	T at level (H_c = 10)	Final T (one pass)	Criterion (H_c = 10)	Criterion (one pass)	$\mu_3^s(t_f)$ (one pass)	$\mu_3^n(t_f)$ (one pass)
3×10^9	49.7663	49.7689 decreasing to 49.7269	0.0037591	0.0037722	3.002×10^9	1.132×10^7
5×10^9	45.3111	45.3101	0.025167	0.025134	5.001×10^9	1.257×10^8
7×10^9	40.9901	40.9896	0.062119	0.062119	7.000×10^9	4.348×10^8
9×10^9	H_c = 15	36.7968 decreasing to 36.7964	H_c = 15	0.11045	9.000×10^9	9.940×10^8
	36.7973		0.11045			

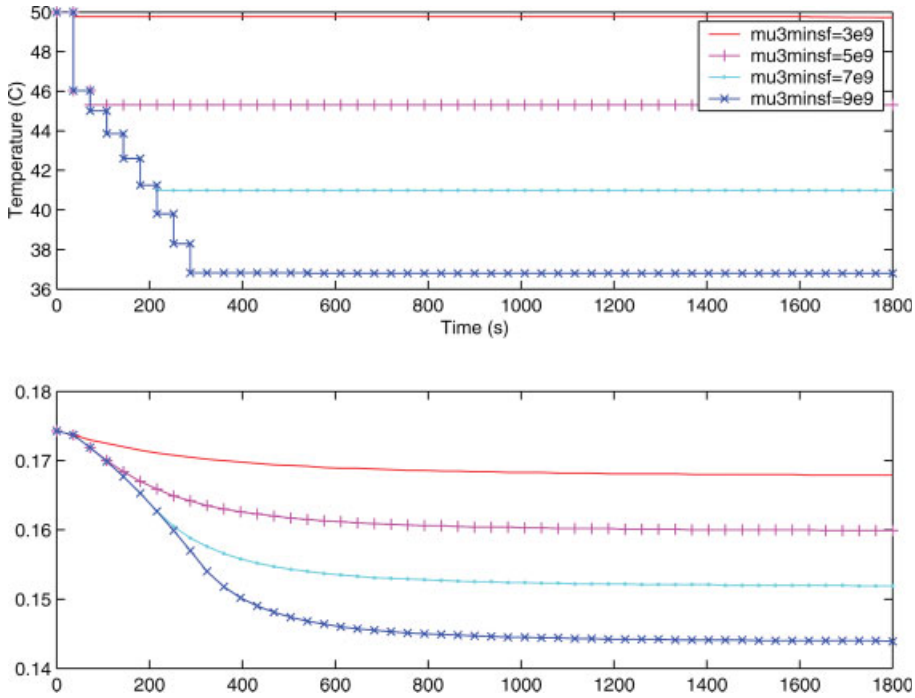

Figure 8. Top: optimal temperature profiles computed in one pass for different values of the final constraint. Bottom: resulting concentration (Objective function: $J=\mu_3^n(t_f)/\mu_3^s(t_f)$ submitted to final constraint $\mu_3^s(t_f) \geq \mu_{3,\min,f}^s$).

[Color figure can be viewed in the online issue, which is available at www.interscience.wiley.com.]

Partial conclusion

In the studied examples, the optimal profile is formed by two arcs separated by a switching time. The first arc where the temperature decreases strongly corresponds to the constraint of the concentration with respect to the metastable concentration, and can be inferred from the implicit relation between the metastable concentration and the temperature. This is a path constraint arc. The type of the second arc depends on the nature of the problem, either the temperature remains at its minimum constraint so that the arc is of input constraint type, or it remains at a level (the value of which depends on the terminal constraint on the third moment, refer to Table 6), where no path or input constraint is satisfied so that this is a sensitivity seeking arc. Thus, even if the nature of the second arc differs, the structure of the optimal profile is the same for all cases. Assuming that the first arc is approximated as a linear temperature decrease, the optimal temperature profile could be parameterized by only two parameters, i.e., the slope of the decreasing line and the switching time. The level temperature of the second arc would result from those values. If the equation of the metastable concentration is known, only one parameter, the switching time, is necessary. For a specialist of crystallization, the first arc is not very surprising, but it is impossible to guess the second arc before making the optimization study. To verify whether the model of the crystallizer has been simplified in an exaggerated manner, and, thus, has some influence on the results which were obtained, a slightly more complicated model is introduced by considering heat exchange with the jacket and further optimization with respect to the temperature of the jacket.

Table 7. $J=\mu_3^n(t_f)/\mu_3^s(t_f)$. Influence of the Value of the Length of the Time Interval on the Level Temperature, on the Criterion for the Constraint Value $\mu_{3,\min,f}^s=7\times10^9$, and on the Mode of Optimization in the Case of One Pass Optimization

	T at level	Criterion $\frac{\mu_3^n s(t_f)}{\mu_3^s(t_f)}$	Characteristics of optimization
Δt = 180s	40.9080	0.066369	Success with initialization at $T_{\max}$
Δt = 90s	40.9811	0.064287	Success with initialization from profile with H_c = 10
Δt = 36s	40.9896	0.062119	Success with initialization at $T_{\max}$
Δt = 18s	40.9922	0.061164	Success only with initialization from profile with H_c = 20

Dynamic Optimization of the Crystallizer with Jacket Heat Exchange

In model (19), the heat exchange between the jacket and the contents of the crystallizer is neglected. A differential equation describing it could be added to model (41) as follows

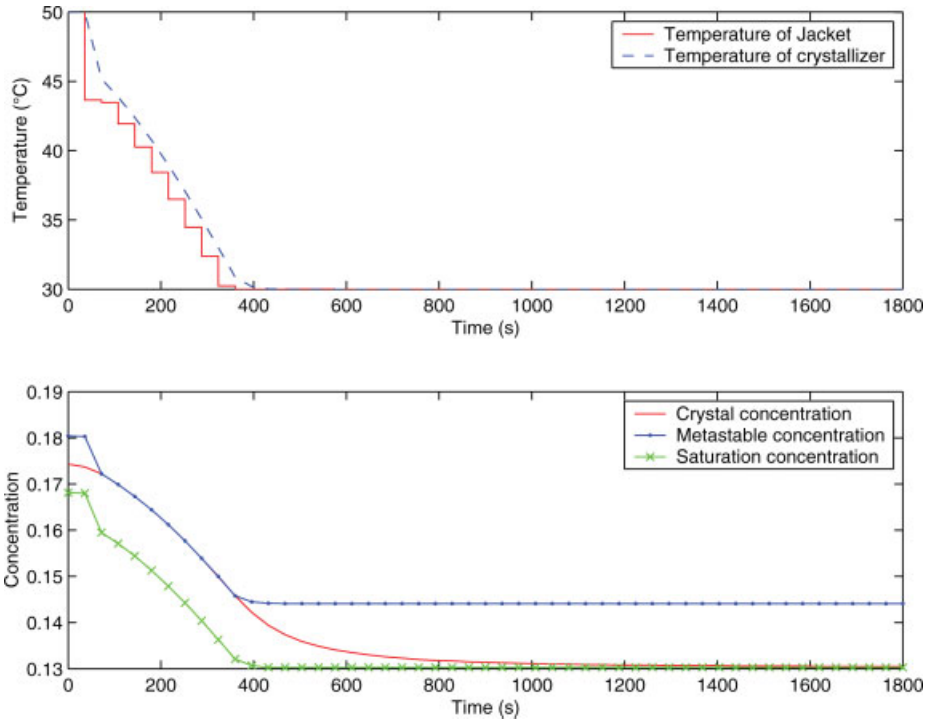

Figure 9. Top: profiles of optimal temperature of the jacket and temperature of the crystallizer (top) computed in one pass for a mass of solvent equal to 3kg. Bottom: corresponding concentration profiles (Objective function: $J=\mu_3^n(t_f)-\mu_3^s(t_f)$).

[Color figure can be viewed in the online issue, which is available at www.interscience.wiley.com.]

$$
\begin{aligned}
\dot{x}_1 &= \dot{C} = -3\rho_c k_v G x_5 \\
\dot{x}_2 &= \dot{T} = \tfrac{UA}{MC_p}(T_j - T) - \tfrac{\Delta H}{C_p} 3\rho_c k_v G x_5 \\
\dot{x}_3 &= \dot{\mu}_0^s = 0 \\
\dot{x}_{3+i} &= \dot{\mu}_i^s = i G x_{3+i-1} \qquad i = 1,3 \\
\dot{x}_7 &= \dot{\mu}_0^n = B \\
\dot{x}_{7+i} &= \dot{\mu}_i^n = i G x_{7+i-1} \qquad i = 1,3 \\
u &= T_j
\end{aligned}
\tag{41}
$$

The heat release due to the newly generated crystals is neglected compared to that of the growing crystals.

For online optimal control, when the model (41) is used, the optimization variable becomes the jacket temperature T_j instead of the crystallizer temperature T. It must be noticed that if the nonlinear term related to the heat of crystallization is neglected in (41), the dynamics between the temperature of the jacket and the temperature of the crystallizer can be represented by a first order transfer function.

The numerical values for the parameters of model (19), except the second differential equation, can be found in Hu et al.[31] The parameters of the second differential equation, i.e., the energy equation for the crystallizer are taken from Sarkar et al.[28]

Case study

The optimization problem with respect to temperature of the jacket is

$$\min_{T_j(t)} J = \mu_3^n(t_f) - \mu_3^s(t_f) \tag{42}$$

subject to model equations (41), initial conditions, constraints (43), (44) and (45). Active nonlinear constraints are set so that the concentration remains between the saturation and metastable limits at any time

$$C_s \le C \le C_m \tag{43}$$

and that the temperature of the crystallizer cannot increase with time

$$\frac{dT}{dt} \le 0 \tag{44}$$

which is a nonlinear constraint. It is furthermore assumed that the optimal temperature of the jacket is limited

$$T_{j,\min} \le T_j \le T_{j,\max} \tag{45}$$

which is a linear constraint in discrete time.

When the energy balance is considered, the model of the system is closer to reality and the value of $T_{j,opt}$ is close to the value of the inlet temperature in the jacket, which can be manipulated in actual practice.[35]

From the energy balance in Equation (41), it appears that the mass M of the crystallizer contents must have an influence on the profile. This has been checked by choosing $M = 3$ similar to Sarkar et al[28] (Figure 9) or $M = 27$ similar to

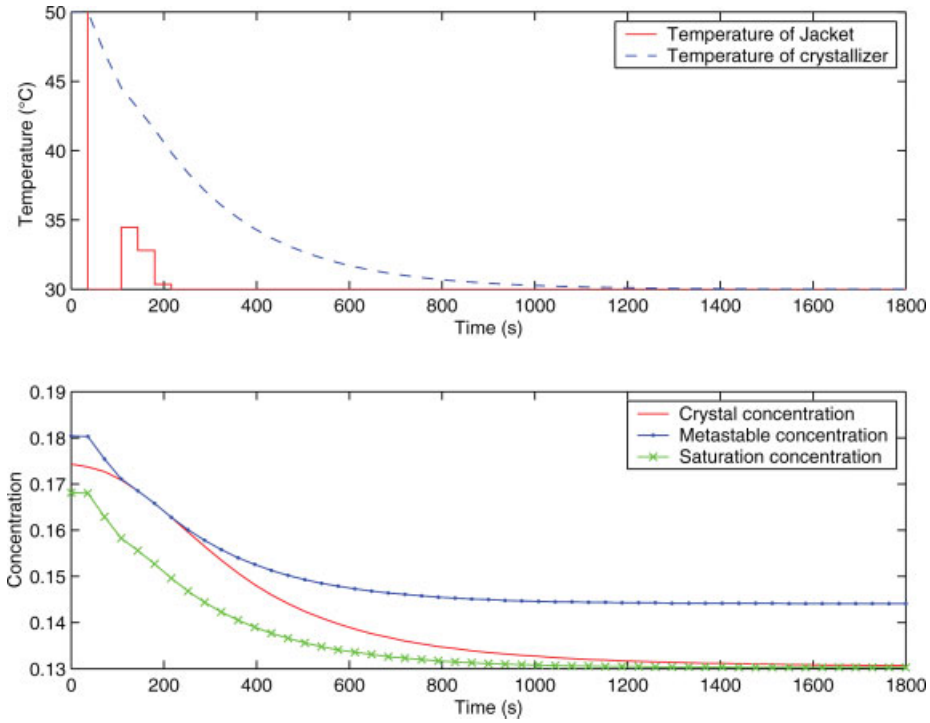

Figure 10. Top: profiles of optimal temperature of the jacket and temperature of the crystallizer computed in one pass for a mass of solvent equal to 27kg. Bottom: corresponding concentration profiles (Objective function: $J=\mu_3^n(t_f)-\mu_3^s(t_f)$).

[Color figure can be viewed in the online issue, which is available at www.interscience.wiley.com.]

Hu et al[31] (Figure 10). These figures should be compared to Figure 1. The influence of the parameter M is very important. If the term of enthalpy of reaction were neglected in the energy balance of Eq. 41, this equation would be equivalent to a continuous first order transfer function of time constant: $\tau=MC_p/(UA)$. For small values of M, the time constant being small, the profiles of the temperature of the crystallizer and of the concentrations are very similar to those found when neglecting the energy balance. Under these conditions, the concentration remains close to the metastable concentration during the decrease of temperature. For the larger mass of solvent, the jacket temperature displays a non monotonous profile (Figure 10) and is often at its minimum value. When M increases, the time constant increases and a lag due to the first order dynamics appears between the temperature of the jacket and the temperature of the crystallizer. In this case, the concentration is close to the metastable concentration only during a short period. The calculated optimal profile of the jacket temperature is more peculiar when M is large, because the crystallizer meets more difficulties to reach its objective, which is to make the concentration close to the metastable concentration. The time to reach the minimum temperature is larger when the dynamics of the jacket is considered. It was found that the increase of the control horizon made the dynamic optimization easier when the parameter M decreased (Table 8). In this Table, the influence of H_c is negligible with regard to the criterion for $M = 27$, whereas the lower values of H_c resulted in bad criteria with $M = 3$. This seems to be due to a large sensitivity of the criterion with respect to an optimal profile of T_j, very close to the minimum constraint $T_{j,\min}$.

On both figures, in case of jacket heat exchange, the concentration needs at least two steps to reach the metastable concentration instead of only one step in absence of this heat exchange. This occurs as first the jacket temperature needs to decrease, then in a second stage it influences the crystallizer temperature, in a way similar to a second-order transfer function.

In the same manner as in case 1, for small M, the profile of optimal resulting temperature is again constituted by two arcs separated by a switching time. However, the first arc is more difficult to be determined as it corresponds to the constraint of the concentration with respect to the metastable concentration, and it must be noted that the optimization

Table 8. Influence of the Value of the Control Horizon on the Criterion

	$H_c = 5$	$H_c = 10$	$H_c = 20$	One pass
Criterion $\mu_3^n(t_f) - \mu_3^s(t_f)$				
for $M = 3$	-9.9515×10^9	-1.0157×10^{10}	-9.8270×10^9	-9.8317×10^9
for $M = 27$	-9.7637×10^9	-9.7629×10^9	-9.7630×10^9	-9.7630×10^9

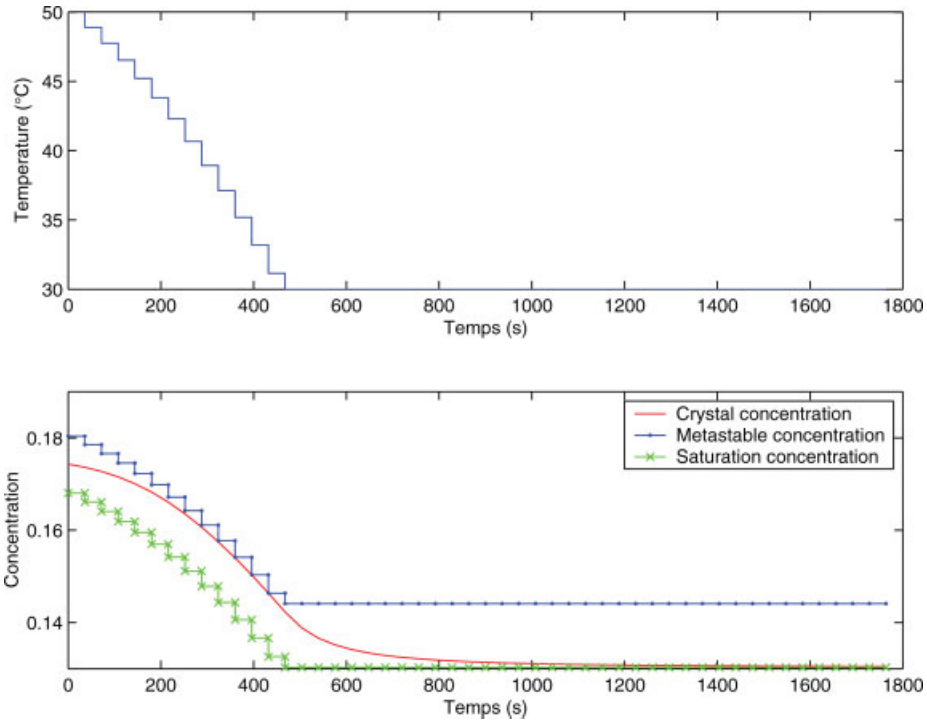

Figure 11. Top: profile of nearly optimal temperature of the crystallizer computed by algorithm ♯1 to be compared to the optimal profile in Figure 1 computed by one pass dynamic optimization. Bottom: corresponding profiles of concentrations to be compared to the concentration in Figure 1 (Objective function: $J=\mu_3^n(t_f)-\mu_3^s(t_f)$ without jacket heat exchange).

[Color figure can be viewed in the online issue, which is available at www.interscience.wiley.com.]

variable is now the jacket temperature, which is not related to the crystallizer temperature by an algebraic equation like (32), but by an ordinary differential equation. The second arc is of input bound type like in case 1. When M is large, the distinction between two arcs is no more visible and a smooth transition occurs.

Partial conclusion

The introduction of the heat exchange between the temperature of the crystallizer and the temperature of the jacket in the model change slightly the results compared to those presented in the principle of receding horizon for dynamic optimization. The model (41) could still be improved by considering the dynamics of the jacket temperature with respect to the inlet jacket temperature. However, this dynamics presents a much smaller time constant than that of the dynamics of the crystallizer temperature with respect to the jacket temperature, and it could nearly be considered as a simple algebraic equation. Per consequent, the new optimal profile would have concerned the inlet temperature in the jacket, but very close results would have been obtained, and the general comments would have been very similar.

A new Quasi-Optimal Temperature Profile without Optimization

The different dynamic optimizations performed previously have shown that the temperature profile is strongly related to the metastable concentration, i.e., first the temperature decreases in order for the concentration of the crystallizer to follow the metastable concentration until the temperature reaches a minimum value. Consequently, it seems that there is a possibility to deduce the temperature profile by a means other than rigorous dynamic optimization. Note that this kind of problem is common in dynamic optimization problems and has been studied in particular by Bonvin and co-workers.[17,18,23] The optimal profile is often constituted of several arcs, some of them being simply described by the constraints, other defined as sensitivity-seeking arcs. The switching times between these arcs are essential parameters for the dynamic optimization problem. Simplified solutions of most dynamic optimization problems can be found by these methods gathered under the concept of necessary conditions of optimality (NCO). In the latter method, the inputs are separated into constraint-seeking and sensitivity-seeking directions.

Rohani and Bourne[50] also proposed a simplified approach to obtain the temperature trajectories in order to achieve constant supersaturation and constant nucleation rate. However, they assumed a perfect model and an Euler approach with a small integration step to solve the model. In this article, although the proposed approach presents similarities, it has been obtained independently by analysis of the characteristics of simplified dynamic optimization such as described in Francois et al.[23] Furthermore, it has been related to model predictive control and real on-line control, which results in a simpler implementation.

From the equation of the metastable concentration C_m, it results

$$\frac{dC_m}{dt} = \frac{\partial C_m}{\partial T}\,\frac{dT}{dt} \Rightarrow \Delta T = \frac{1}{\frac{\partial C_m}{\partial T}}\,\frac{dC_m}{dt}\Delta t \tag{46}$$

where Δt is a finite time step corresponding to a sampling period, and ΔT the corresponding temperature increment. The next idea is to force C to follow C_m, as it was noticed in case 1. Thus, in the expression of the growth rate, C is replaced by C_m. The rest of the algorithm is simply obtained by first-order discretization of a reduced set of differential equations taken from (19). In spite of its well-known inacurracy, Euler-type discretization is voluntarily chosen here to play the same role as piecewise-constant control for a controlled process in order to demonstrate the idea. However, the differential equations could have been maintained, as in the original model by just adding the constraint $C=C_m$, which would transform the differential system into a differential-algebraic system. Note that the size of the reduced model does not depend on the objective function, as only the second-order moment is needed in the derivative of the concentration. The objective function is to be calculated separately by any rigorous numerical method of integration of the full set of equations.

The first algorithm is first shown for case 1, without heat exchange, without final constraint which is simpler. The principle is the following:

Algorithm ♯1 for approximate optimal profile (case 1) without jacket heat exchange:

a1. $k = 0$. Initialize temperature, concentration, metastable and saturation concentrations, moments, and growth rate.
a2. Start of iterative sequence: k=k+1
a3. $t(k+1)=t(k)+\Delta t$
a4. Calculate $C_s(k), C_m(k)$
a5. $G(k)=k_{g0}\exp\left(-\frac{E_g}{RT(k)}\right)\left(\frac{C(k)-C_s(k)}{C_s(k)}\right)^g$
a6. $G_{forced}(k)=k_{g0}\exp\left(-\frac{E_g}{RT(k)}\right)\left(\frac{C_m(k)-C_s(k)}{C_s(k)}\right)^g$
a7. Calculate $\frac{\partial C_m}{\partial T}(k)$
a8. $\frac{dC}{dt}(k)=-3\rho_c k_v G(k)\mu_2(k)$
a9. $\left(\frac{dC}{dt}\right)_{forced}(k)=-3\rho_c k_v G_{forced}(k)\mu_2(k)$
a10. $\Delta T(k)=\frac{1}{\frac{\partial C_m}{\partial T}(k)}\left(\frac{dC}{dt}\right)_{forced}(k)\Delta t$
a11. $T(k+1)=T(k)+\Delta T(k)$
a12. If $T(k+1)<T_{\min}$, Then $T(k+1)=T_{\min}$
a13. $C(k+1)=C(k)+\frac{dC}{dt}(k)\Delta t$
a14. $\mu_0(k+1)=\mu_0(k)$
a15. $\mu_1(k+1)=\mu_1(k)+G(k)\,\mu_0(k)\,\Delta t$
a16. $\mu_2(k+1)=\mu_2(k)+2\,G(k)\,\mu_1(k)\,\Delta t$
a17. If $t \geq t_f$, Then End, Else go back to a2.

where t is time at iteration k, Δt is time step, $C_s(k)$ and $C_m(k)$ are the metastable and saturation concentrations, $T(k)$ is the crystallizer temperature, $C(k)$ is the concentration, $T_{\min}$ is the minimum temperature, G is the growth rate, μ_0, μ_1, μ_2 are moments.

As such, the algorithm ♯1 is adapted to case study 1. Note that it does not require the calculation of the third moments which are present in criterion (29).

The simulation result of algorithm ♯1 is shown in Figure 11. It appears that very similar results to those of Figure 1 are obtained although the latter Figure needed nonlinear optimization to solve the dynamic optimization problem. The temperature profile obtained by the algorithm ♯1 is less stiff than the one obtained by dynamic optimization, but the simple Euler discretization with $\Delta t=36$ has largely contributed to that difference. In particular, the time to reach the metastable concentration is longer as it was reached in one step in the case of dynamic optimization. Note that for algorithm ♯1, because of our particular intention to reduce all the calculations, the values of concentrations which are shown are obtained by the simple Euler "integration" of the algorithm, and are not equal to the actual values that would result from a rigorous integration. Thus, they should be considered more as a tendency. In an experimental case study, measurements could be used instead of calculated values.

For case studies 2 and 3, constraints (30) or (40) must be respected, respectively. In the following, for cases 2 and 3, slight modifications of the algorithm are proposed.

Algorithm ♯2 for approximate optimal profile (cases 2 and 3) without jacket heat exchange, but with final constraint:

Lines a1 to a16 remain the same as in algorithm ♯1.
a17. $\mu_3(k+1)=\mu_3(k)+3\,G(k)\,\mu_2(k)\,\Delta t$
a18. Estimation of $\hat{\mu}_3(N)$ by inner loop on $i=k+1,\ldots,N$ assuming that $T(i)=T(k+1)$
a19. If $\hat{\mu}_3(N) \geq \mu^s_{3,\min_f}$, Then $\Delta T(k)=0$, $T(k+1)=T(k)$
a20. If $t \geq t_f$, Then End, Else go back to a2.

Algorithm ♯2 has been tested for case study 2 (Objective function: $J=\mu^n_3(t_f)$ submitted to constraint $\mu^s_3(t_f) \geq 8.33 \times 10^9$). Due to the final constraint on $\mu^s_3(t_f)$, if $\mu^s_3(k+1)$ were used for comparison to the final constraint, this would be the cause of a large error because of the evolution of μ^s_3, in the time interval $[k+1,N]$, so that the construction of a simple estimator of $\mu^s_3(t_f)$ is necessary. The estimator is calculated by an inner loop initiated at time $k+1$ by the actual value of $\mu^s_3(k+1)$, assuming that the temperature is constant on $[k=1,N]$ and that the growth, concentration, and all moments vary on this interval according to previous Euler variations. This estimation leads to $\hat{\mu}^s_3(N)=8.85 \times 10^9$, and a level temperature of 37.1055 (Figure 12) compared to the respective final value of $\mu^s_3(t_f)=8.33 \times 10^9$, and level temperature of 38.1878 obtained by rigorous one pass optimization. These results are considered as satisfactory for this simplified algorithm.

In the case of jacket heat exchange and for criterion (42), the algorithm ♯1 can be simply modified by use of the jacket heat exchange equation as follows.

Algorithm ♯3 for approximate optimal profile with jacket heat exchange, without final constraint:

Lines a1 to a12 remain the same as in algorithm ♯1.
a13. $T_j(k)=T(k)+\frac{M}{UA}\left[\Delta H 3\rho_c k_v G(k)\mu_2(k)+C_p\frac{\Delta T}{\Delta t}\right]$
a14. $C(k+1)=C(k)+\frac{dC}{dt}(k)\Delta t$
a15. $\mu_0(k+1)=\mu_0(k)$
a16. $\mu_1(k+1)=\mu_1(k)+G(k)\,\mu_0(k)\,\Delta t$
a17. $\mu_2(k+1)=\mu_2(k)+2\,G(k)\,\mu_1(k)\,\Delta t$
a18. If $t \geq t_f$, Then End, Else go back to a2.

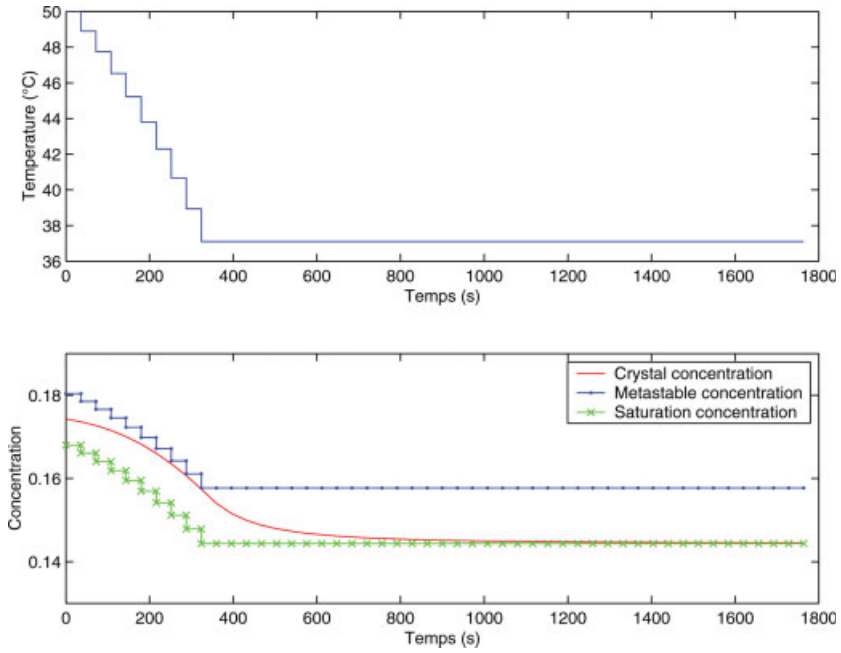

Figure 12. Top: profile of nearly optimal temperature of the crystallizer computed by algorithm ♯2 to be compared to the optimal profile in Figure 3 computed by one pass dynamic optimization. Bottom: corresponding profiles of concentrations to be compared to the concentration in Figure 3 (Objective function: $J=\mu_3^n(t_f)$ submitted to constraint $\mu_3^s(t_f) \geq 8.33 \times 10^9$ without jacket heat exchange).

[Color figure can be viewed in the online issue, which is available at www.interscience.wiley.com.]

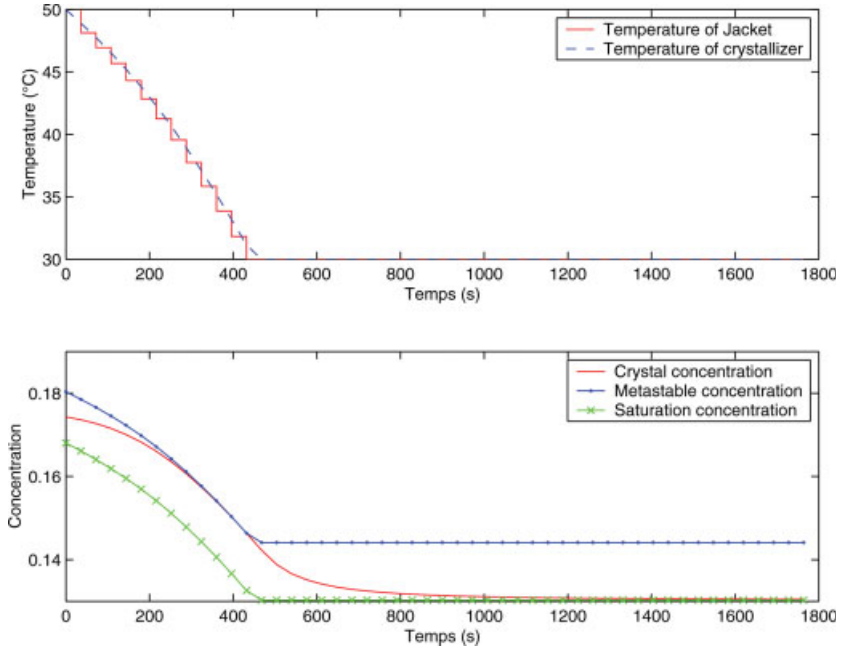

Figure 13. Top: profile of nearly optimal temperature of the crystallizer computed by algorithm ♯3 to be compared to the optimal profile in Figure 9 computed by one pass dynamic optimization with a receding horizon equal to 3. Bottom: corresponding profiles of concentrations to be compared to the concentration in Figure 9 (Objective function: $J=\mu_3^n(t_f)-\mu_3^s(t_f)$ with jacket heat exchange and M=3kg).

[Color figure can be viewed in the online issue, which is available at www.interscience.wiley.com.]

In this latter version ♯3 of the quasi-optimal algorithm, the manipulated variable is the jacket temperature $T_j(k)$ which thus provides the optimal profile. Compared to the rigorous results of Figure 9, the algorithm ♯3 provokes a slightly exagerated decrease of the crystallizer temperature which crosses the jacket temperature (Figure 13). However, like in case of both previous algorithms, the crystallizer temperature, which is here indicated results from the simple Euler "integration", used by the algorithm and does not represent the actual or "measured" value, which would have resulted from rigorous integration. The crystallizer concentration joins the constraint with respect to the metastable concentration on a lower portion of time than in rigorous optimization.

Note that, in algorithms ♯1 and ♯3, where no final constraint intervenes, only a reduced model is necessary compared to the full model represented by Eq. 41. The case of ♯2 with final constraint obliged us to construct a simplified estimator. The authors think that the present method is in particular well adapted to industrial applications where a quasi-optimal profile is sufficient. In order to improve the robustness, more advanced methods, including an observer such as the extended Kalman filter, could be used to take into account the actual measurements of temperature[51] instead of predicted temperatures. Considered alone, i.e., in absence of feedback control, due to its structure, the observer is sufficient to correct the trajectory.

Conclusion

A simplified method inspired from non linear model predictive control or receding horizon has been first introduced and tested on different objective functions with various constraints in order to solve the non linear dynamic optimization problems for a batch crystallizer. It gives excellent results with no appreciable difference from those obtained by rigorous dynamic optimization, is more easily implementable and much faster. Furthermore, it has been shown that if full dynamic optimization fails because of an excessive number of optimized variables, the receding horizon optimization proposed in this article can be used as a successfull start in order to later facilitate the dynamic optimization. When the heat exchange between the crystallizer contents and the jacket is considered, the dynamics of the cooling jacket exerts an increasing influence on the optimal profiles with the mass of the crystallizer contents. In a general way, it was demonstrated that the optimal profile is composed of several arcs either related to inputs bounds, path constraints, or sensitivity seeking, which are separated by switching instants. The dynamic optimization procedure can be thought very differently from traditional approaches and could be solved in an iterative manner especially in real applications. These remarks finally led the authors to propose simple algorithms related to online control, which allow us to find quasi-optimal temperature profiles provided that the type and sequence of arcs have been previously determined. This method is well adapted to industrial situations.

Notation

A = surface area of heat transfer, m^2
B = nucleation rate, number/kg solvent/s
C = concentration, kg solute/kg solvent
C_m = metastable concentration, kg solute/kg solvent
C_p = heat capacity at constant pressure, $J.kg^{-1}.K^{-1}$
C_s = saturated concentration, kg solute/kg solvent
E = activation energy, $J.mol^{-1}$
G = growth rate, $m.s^{-1}$
H_c = control horizon in terms of sampling periods
k = kinetic constant
k_v = volume shape factor
M = mass, kg
R = universal gas constant, $J.mol^{-1}.K^{-1}$
r = radius of crystals, m
t = time, s
T = temperature, °C
T_s = sampling period, s
u = manipulated variable
U = heat-transfer coefficient, $W.m^{-2}K^{-1}$
x = State

Greek letters

ΔH = Heat of crystallization, $J.kg^{-1}$
$\mu_i = i^{th}$ order moment
ρ_c = crystal density, $kg.m^{-3}$

Subscripts and superscripts

b = nucleation
f = final
g = growth
j = jacket
n = nucleated crystals
s = seeded crystals

Literature Cited

1. Randolph A, Larson M. *Theory of particulate processes*. New York: Academic Press. 1971.
2. Ajinkya M, Ray W. On the optimal operation of crystallization processes. *Chem Eng Comm*. 1974;1:181–186.
3. Choong K, Smith R. Optimization of batch cooling crystallization. *Chem Eng Sci*. 2004;59:313–327.
4. Choong K, Smith R. Novel strategies for optimization of batch, semi-batch and heating/cooling evaporative crystallization. *Chem Eng Sci*. 2004;59:329–343.
5. Costa C, Filho R. Evaluation of optimisation techniques and control variable formulations for a batch cooling crystallization process. *Chem Eng Sci*. 2005;60:5312–5322.
6. Jones A. Optimal operation of a batch cooling crystallizer. *Chem Eng Sci*. 1974;29:1075–1087.
7. Lang Y, Cervantes A, Biegler L. Dynamic optimization of a batch cooling crystallization process. *Ind Eng Chem Res*. 1999;38:1469–1477.
8. Miller S, Rawlings J. Model identification and control strategies for batch cooling crystallizers. *AIChEJ*. 1994;40:1312–1327.
9. Rawlings J, Slink C, Miller S. Model identification and control of solution crystallization process: A review. *Ind Eng Chem Res*. 1993;32:1275–1296.
10. Kubota N, Doki N, Yokota M, Sato A. Seeding policy in batch cooling crystallization. *Powder Technol*. 2001;121:31–38.
11. Marchal P, David R, Klein J, Villermaux J. Crystallization and precipitation engineering - I. An efficient method for solving population balance in crystallization with agglomeration. *Chem Eng Sci*. 1988;43:59–67.
12. Luus R. Optimal control of bath reactors by Iterative Dynamic Programming. *J Proc Cont*. 1994;4(4):218–226.
13. Fliess M, Lévine J, Martin P, Rouchon P. Flatness and defect of nonlinear systems: introductory theory and examples. *Int J Cont*. 1995;61:1327–1361.
14. Vollmer U, Raisch J. Control of batch cooling crystallization processes based on orbital flatness. *Int J Cont*. 2003;76:1635–1643.
15. Guay M. An algorithm for orbital feedback linearization of single-input control affine systems. *Syst Cont Lett*. 1999;38:271–281.

16. Ma D, Chung S, Braatz R. Worst-case performance analysis of optimal batch control trajectories. *AIChE J*. 1999;45(7):1469–1476.
17. Srinivasan B, Palanki S, Bonvin D. Dynamic optimization of batch processes. I. Characterization of the nominal solution. *Comp Chem Eng*. 2003;27:1–26.
18. Srinivasan B, Bonvin D, Visser E, Palanki S. Dynamic optimization of batch processes. II. Roles of measurements in handling uncertainty. *Comp Chem Eng*. 2003;27:27–44.
19. Srinivasan B, Bonvin D. Controllability and stability of repetitive batch processes. *J Process Cont*. 2007;17:285–295.
20. Visser E, Srinivasan B, Palanki S, Bonvin D. A feedback-based implementation scheme for batch process optimization. *J Process Control*. 2000;(10):399–410.
21. Srinivasan B, Primus C, Bonvin D, Ricker N. Run-to-run optimization via control of generalized constraints. *Cont Eng Pract*. 2001;9:911–919.
22. Srinivasan B, Bonvin D. Real-time optimization of batch processes by tracking the necessary conditions of optimality. *Ind Eng Chem Res*. 2007;46(2):492–504.
23. Francois G, Srinivasan B, Bonvin D. Use of measurements for enforcing the necessary conditions of optimality in the presence of constraints and uncertainty. *J Proc Cont*. 2005;15:701–712.
24. Kadam J, Schlegel M, Srinivasan B, Bonvin D, Marquardt W. Dynamic optimization in the presence of uncertainty: from off-line nominal solution to measurement-based implementation. *J Proc Cont*. 2007;17:389–398.
25. Bryson A, Ho Y. *Applied Optimal Control*. Washington: Hemisphere; 1975.
26. Logsdon J, Biegler L. Accurate solution of differential-algebraic optimization problems. *Ind Eng Chem Res*. 1989;28:1628–1639.
27. Chung S, Ma D, Braatz R. Optimal seeding in batch crystallization. *Can J Chem Eng*. 1999;77:590–596.
28. Sarkar D, Rohani S, Jutan A. Multi-objective optimization of seeded batch crystallization processes. *Chem Eng Sci*. 2006;61:5282–5295.
29. Deb K, Pratap A, Agarwal S, Meryarivan T. A fast and elitist multiobjective genetic algorithm: NSGA-II. *IEEE Trans Evolution Comput*. 2002;6:182–197.
30. Zhang G, Rohani S. On-line optimal control of a seeded batch crystallizer. *Chem Eng Sci*. 2003;58:1887–1896.
31. Hu Q, Rohani S, Jutan A. Modelling and optimization of seeded batch crystallizers. *Comp Chem Eng*. 2005;29:911–918.
32. Hu Q, Rohani S, Jutan A. New numerical method for solving the dynamic population balance equations. *AIChEJ*. 2005;51:1–7.
33. Hu Q, Rohani S, Wang DX, Jutan A. Optimal control of a batch cooling seeded crystallizer. *Powder Technol*. 2005;156:170–176.
34. Bryson A. *Dynamic Optimization*. Menlo Park, California: Addison Wesley; 1999.
35. Corriou JP. *Process Control - Theory and Applications*. London: Springer Verlag; 2004.
36. Pontryagin L, Boltyanskil V, Gamkrelidge R, Mishchenko E. *The mathematical theory of optimal processes* New York: Interscience; 1962.
37. Teo K, Goh C, Wong K. *A Unified Computational Approach to Optimal Control Problems*. Wiley and Sons, Inc., New York; 1991.
38. Maciejowski J. *Predictive Control*. Harlow, U.K.: Pearson Education; 2002.
39. Bemporad A, Morari M, Dua V, Pistikopoulos E. The explicit linear quadratic regulator for constrained systems. *Automatica*. 2002;38:3–20.
40. Bartlett R, Biegler L, Backstrom J, Gopal V. Quadratic programming algorithms for large-scale model predictive control. *J Process Control*. 2002;12:775–795.
41. Zheng A. Nonlinear model predictive control, chap. *Practical issues and possible solutions for NMPC*. Basel: Birkhäuser; 2000;129–144.
42. Schittkowski K. NLPQL: A Fortran subroutine solving constrained nonlinear programming problems. *Ann Oper Res*. 1985;5:485–500.
43. Shi D, El-Farra N, Li M, Mhaskar P, Christofides P. Predictive control of particle size distribution in particulate processes. *Chem Eng Sci*. 2006;61:268–281.
44. Petzold L. Automatic selection of methods for solving stiff and nonstiff systems of ordinary differential equations. *Siam J Sci Stat Comput*. 1983;4:136–148.
45. Hindmarsh A. *Odepack, a systematized collection of ode solvers, in scientific computing*. Amsterdam: North-Holland; 1983;55–64.
46. Goh C, Teo K. Control parametrization: a unified approach to optimal control problems with general constraints. *Automatica*. 1988;24(1):3–18.
47. Serban R, Hindmarsh A. CVODES: an ODE solver with sensitivity analysis capabilities. *Ucrl-jp-200039*, Lawrence Livermore Laboratory; 2003
48. Petzold L, Li S, Cao Y, Serban R. Sensitivity analysis of differential-algebraic equations and partial differential equations. *Tech. rep*., Lawrence Livermore Laboratory; 2006.
49. Isidori A. *Nonlinear Control Systems*. 3rd ed. New York: Springer-Verlag; 1995.
50. Rohani S, Bourne J. A simplified approach to the operation of a batch crystallizer. *Can J Chem Eng*. 1990;68:799–806.
51. Corriou JP, Rohani S. Nonlinear control of a batch crystallizer. *Chem Eng Comm*. 2002;189(10):1415–1436.

Manuscript received Jun. 15, 2007, and revision received July 8, 2008.